Inorg. Chem. **2008**, *47*, 3661−3668

Synthesis and Molecular and Electronic Structures of a Series of Mo_3CoSe_4 Cluster Complexes with Three Different Metal Electron Populations

Antonio Alberola,[†] Rosa Llusar,*[,†] Cristian Vicent,[‡] Juan Andrés,[†] Victor Polo,[†] and Carlos J. Gómez-García[§]

Departament de Química Física i Analítica, Universitat Jaume I, Av. Sos Baynat s/n, 12071 Castelló, Spain, Serveis Centrals d'Instrumentació Científica, Universitat Jaume I, Av. Sos Baynat s/n, 12071 Castelló, Spain, and Instituto de Ciencia Molecular, Universitat de Valencia, Instituto de Ciencia Molecular, Polígono la Coma s/n, E-46980, Paterna, Spain

Received November 9, 2007

The synthesis, crystal structure, and magnetic properties of $[Mo_3(CoCO)Se_4(dmpe)_3Cl_3]$ (**1**), $[Mo_3(CoCl)Se_4(dmpe)_3Cl_3]$ (**2**), and $[Mo_3(CoCl)Se_4(dmpe)_3Cl_3](TCNQ)$ ([**2**](TCNQ)) (dmpe = 1,2-bis(dimethylphosphanyl)ethane; TCNQ = 7,7,8,8-tetracyanoquinomethane) cubane-type complexes with 16, 15, and 14 metal electrons, respectively, are reported. These compounds complete the series of cobalt-containing Mo_3CoQ_4 (Q = S, Se) cubane-type complexes, which allows a complete analysis of the consequences of replacing the inner chalcogen and the metal electron count on the structural, magnetic, and electrochemical properties. The experimental evidence is theoretically supported and rationalized on the basis of density-functional theory calculations. For the 15-metal electron $[Mo_3(CoCl)Se_4(dmpe)_3Cl_3]$ complex with $S = {}^1/_2$, both electron paramagnetic resonance and theoretical studies give support to a spin density mainly located on the heteroatom. The nature of the highest occupied molecular orbital upon chalcogen exchange within the Mo_3CoQ_4 (Q = S, Se) series remains essentially unchanged, whereas the nature of the ligand attached to Co (Cl or CO) results in a different ordering of the molecular orbital scheme. This behavior is explained by the absence of backdonation between an occupied d orbital of Co to an empty π^* Cl orbital, to yield frontier orbitals that differ from those of previous models.

Introduction

Group VI transition metal cluster chalcogenides constitute a large and rapidly growing family of inorganic compounds with applications in multidisciplinary fields. Representative examples are the molybdenum chalcogenides, so-called chevrel phases $A_xMo_6Q_8$ (A = alkali, transition, and rare earth metals; Q = S, Se, Te; $x = 0$–4) with unusual physical properties such as ion conduction,[1] themoelectricity,[2] hydrodesulfurization catalysis,[3] or superconductivity.[4] Sulfur-rich triangular Mo_3S_7 complexes are also known, and their use in the development of molecular conductors[5–7] and nonlinear optical materials is well-documented.[8] Another category of group VI cluster chalcogenides is that containing a $M_3M'Q_4$ (M = Mo, W; Q = S, Se; M′ = transition or post-transition metal) cubane-type structure, where the metal and chalcogen atoms occupy adjacent vertices in a cube. Unique reactivities of the heterometal (transition or noble metal centers denoted as M′) embedded in the robust and redox-active cubane-type $M_3M'Q_4$ cores have been reported. For example, cuboidal Mo_3PdS_4 cores catalyze the addition

* To whom correspondence should be addressed. Fax: (+34)-964728066. Tel.: (+34)-964728086. E-mail: Rosa.Llusar@qfa.uji.
† Departament de Química Física i Analítica, Universitat Jaume I.
‡ Serveis Centrals d'Instrumentació Científica, Universitat Jaume I.
§ Universitat de Valencia.

(1) Schollhorn, R. *Angew. Chem., Int. Ed.* **1980**, *19*, 983.
(2) Nunes, R. W.; Mazin, I. I.; Singh, D. J. *Phys. Rev. B: Condens. Matter Mater. Phys.* **1999**, *59*, 7969.
(3) Benson, J. W.; Schrader, G. L.; Angelici, R. J. *J. Mol. Catal.* **1995**, *96*, 283.
(4) Seeber, B.; Decroux, M.; Fischer, O. *Physica B* **1989**, *155*, 129.
(5) Llusar, R.; Uriel, S.; Vicent, C.; Clemente-Juan, J. M.; Coronado, E.; Gómez-Garcia, C. J.; Braida, B.; Canadell, E. *J. Am. Chem. Soc.* **2004**, *126*, 12076.
(6) Llusar, R.; Triguero, S.; Uriel, S.; Vicent, C.; Coronado, E.; Gómez-Garcia, C. J. *Inorg. Chem.* **2005**, *44*, 1563.
(7) Alberola, A.; Llusar, R.; Triguero, S.; Vicent, C.; Sokolov, M. N.; Gomez-Garcia, C. *J. Mater. Chem.* **2007**, *17*, 3440.
(8) Garriga, J. M.; Llusar, R.; Uriel, S.; Vicent, C.; Usher, A. J.; Lucas, N. T.; Humphrey, M. G.; Samoc, M. *Dalton Trans.* **2003**, 4546.

10.1021/ic7022083 CCC: $40.75
Published on Web 03/21/2008

of methanol or carboxylic acids to electron-deficient alkynes;[9–11] $Mo_3M'S_4$ is an efficient catalyst in hydrodesulfurization reactions (M′ = Ni)[12,13] and promotes the intermolecular cyclopropanation of alkenes with ethyl diazoacetate (M′ = Cu).[14] In these reactions, it can be assumed that the putative mechanistic picture proceeds with the cuboidal $Mo_3M'S_4$ core cycling through several oxidation states during turnover. However, the isolation of the $Mo_3M'S_4$ series with different electron counting is rarely achieved in contrast with the versatile electrochemistry displayed by their homometallic M_4Q_4 (M = Mo, W; Q = S, Se) counterparts.[15–17] For example, Mo_3NiS_4 or Mo_3FeS_4 compounds are invariably isolated as 16- and 14-metal-electron species, respectively,[18,19] whereas for copper-containing Mo_3CuS_4 clusters, species possessing 16 and 17 metal electrons have been structurally characterized.[20,21] Fundamental input aimed at validating theoretical descriptions can be obtained by analysis of the structural and spectroscopic consequences of electron addition and removal within an isostructural $Mo_3M'S_4$ series, although its synthesis and isolation remains a challenge from a synthetic point of view.

Recently, we have shown that cobalt incorporation into preassembled Mo_3S_4 complexes allows the isolation of the first series of Mo_3CoS_4 clusters with three different metal electron populations.[22] Herbst et al. have also prepared a closely related series of Mo_3CoS_4 complexes bearing cyclopentadienyl ligands with four different metal electron counts, although only the 14-metal-electron derivative has been structurally characterized.[23,24] In all cases, the choice of the ligand attached to the cobalt is crucial to obtain a certain Mo_3CoS_4 cluster. Other Mo_3CoS_4 cubane-type complexes bearing aqua ligands have been reported, and their redox interconversion has been investigated using spectroscopic techniques.[25–27]

In general, the chemical development of group VI cluster chalcogenides has been mainly focused on the sulfur derivatives, while minor attention has been paid to the selenide and teluride homologues. This is partially due to the less-developed synthetic routes available for the Se or Te complexes. The more evident strategy for the preparation of chalcogenide (Se, Te) group VI complexes relies on the adaptation of the synthetic procedures previously described for the sulfur homologues. This approach has been successfully employed for the preparation of various $M_3M'Se_4$ cubane-type complexes.[28–30] In this context, the preparation of complete series of cluster chalcogenides, where the S, Se, or Te can be systematically incorporated, is instructive in order to complement the knowledge of the most commonly found sulfur derivatives. Chalcogen replacement within a homologous series of group VI chalcogenide complexes has been used to fine-tune the electrochemical,[31,32] nonlinear optical properties[33] as well as the kinetics of ligand substitution in molecular M_3Q_4 complexes,[34,35] or the kinetics of intercalation of divalent cations in chevrel phases.[36,37]

Herein, we report the adapted synthesis of the series of Mo_3CoS_4 clusters with three different populations to their selenium analogues. In this way, the successful preparation of a complete family of Mo_3CoQ_4 (Q = S, Se) cluster complexes in which either the electronic population or the identity of the inner chalcogenide can be modified provides a unique scenario where the structural, electronic, magnetic, or redox properties can be systematically evaluated. The understanding of such observed phenomena can be further improved by means of accurate density functional theory (DFT) calculations, which provide direct information about changes in the geometrical parameters or the localization of unpaired spin density obtained from the analysis of the electronic structure for the experimentally studied clusters.

(9) Murata, T.; Gao, H.; Mizobe, Y.; Nakano, F.; Motomura, S.; Tanase, T.; Yano, S.; Hidai, M. *J. Am. Chem. Soc.* **1992**, *114*, 8287.
(10) Murata, T.; Mizobe, Y.; Gao, H.; Ishii, Y.; Wakabayashi, T.; Nakano, F.; Tanase, T.; Yano, S.; Hidai, M.; Echizen, L.; Nanikawa, H.; Motomura, S. *J. Am. Chem. Soc.* **1994**, *116*, 3389.
(11) Wakabayashi, T.; Ishii, Y.; Ishikawa, K.; Hidai, M. *Angew. Chem., Int. Ed.* **1996**, *108*, 2268.
(12) Schmidt, I.; Hyldoft, J.; Hjortkjaer, J.; Jacobsen, C. J. *Acta Chim. Scand.* **1996**, *50*, 871.
(13) Feliz, M.; Llusar, R.; Uriel, S.; Vicent, C.; Brorson, M.; Herbst, K. *Polyhedron* **2005**, *24*, 1212.
(14) Feliz, M.; Guillamon, E.; Llusar, R.; Vicent, C.; Stiriba, S. E.; Perez-Prieto, J.; Barberis, M. *Chem.—Eur. J.* **2006**, *12*, 1486.
(15) Shibahara, T. *Coord. Chem. Rev.* **1992**, *123*, 73.
(16) McFarlane, W.; Nasreldin, M.; Saysell, D. M.; Jia, Z. S.; Clegg, W.; Elsegood, M. R. J.; Murray, K. S.; Moubaraki, B.; Sykes, A. G. *J. Chem. Soc., Dalton Trans.* **1996**, 363.
(17) Sokolov, M.; Esparza, P.; Hernandez-Molina, R.; Platas, J. G.; Mederos, A.; Gavin, J. A.; Llusar, R.; Vicent, C. *Inorg. Chem.* **2005**, *44*, 1132.
(18) Shibahara, T.; Sakane, G.; Naruse, Y.; Taya, K.; Akashi, H.; Ichimura, A.; Adachi, H. *Bull. Chem. Soc. Jpn.* **1995**, *68*, 2769.
(19) Shibahara, T.; Akashi, H.; Kuroya, H. *J. Am. Chem. Soc.* **1986**, *108*, 1342.
(20) Hegetschweiler, K.; Wörh, M.; Meienberger, M. D.; Nesper, R.; Schmalle, H. W.; Hancock, R. D. *Inorg. Chim. Acta* **1996**, *250*, 35.
(21) Feliz, M.; Garriga, J. M.; Llusar, R.; Uriel, S.; Humphrey, M. G.; Lucas, N. T.; Samoc, M.; Luther-Davies, B. *Inorg. Chem.* **2001**, *40*, 6132.
(22) Feliz, M.; Llusar, R.; Uriel, S.; Vicent, C.; Coronado, E.; Gómez-Garcia, C. *Chem.—Eur. J.* **2004**, *10*, 4308.
(23) Curtis, M. D.; Riaz, U.; Curnow, O. J.; Kampf, J. W. *Organometallics* **1995**, *14*, 5337.
(24) Herbst, K.; Soderhjelm, E.; Nordlander, E.; Dahlenburg, L.; Brorson, M. *Inorg. Chim. Acta* **2007**, *360*, 2697.
(25) Shibahara, T.; Akashi, H.; Yamasaki, M.; Hashimoto, K. *Chem. Lett.* **1991**, 689.
(26) Dimmock, P. W.; Saysell, D. M.; Sykes, A. G. *Inorg. Chim. Acta* **1994**, *225*, 157.
(27) Hernandez-Molina, R.; Sykes, A. G. *Coord. Chem. Rev.* **1999**, *187*, 291.
(28) Hernandez-Molina, R.; Sokolov, M.; Esparza, P.; Vicent, C.; Llusar, R. *Dalton Trans.* **2004**, 847.
(29) Llusar, R.; Uriel, S.; Vicent, C. *J. Chem. Soc., Dalton Trans.* **2001**, 2813.
(30) Hernandez-Molina, R.; Sokolov, M.; Clausen, M.; Clegg, W. *Inorg. Chem.* **2006**, *45*, 10567.
(31) Feliz, M.; Llusar, R.; Uriel, S.; Vicent, C.; Humphrey, M. G.; Lucas, N. T.; Samoc, M.; Luther-Davies, B. *Inorg. Chim. Acta* **2003**, *349*, 69.
(32) Mishra, L.; Vilaplana, R.; Singh, V. K.; Yadaw, A. K.; Gonzalez-Vilchez, F. *J. Inorg. Biochem.* **2001**, *86*, 581.
(33) Zhang, Q.-F.; Leung, W.-H.; Xin, X. *Coord. Chem. Rev.* **2002**, *224*, 35.
(34) Basallote, M. G.; Estevan, F.; Feliz, M.; Fernandez-Trujillo, M. J.; Hoyos, D. A.; Llusar, R.; Uriel, S.; Vicent, C. *Dalton Trans.* **2004**, 530.
(35) Saysell, D. M.; Fedin, V. P.; Lamprecht, G. J.; Sokolov, M. N.; Sykes, A. G. *Inorg. Chem.* **1997**, *23*, 2982.
(36) Gocke, E.; Schramm, W.; Dolscheid, P.; Schollhorn, R. *J. Solid State Chem.* **1987**, *70*, 71.
(37) Levi, E.; Lancry, E.; Mitelman, A.; Aurbach, D.; Ceder, G.; Morgan, D.; Isnard, O. *Chem. Mater.* **2006**, *18*, 5492.

In addition, useful chemical concepts and bonding schemes based on molecular orbitals (MOs) can be derived in order to rationalize the changes observed upon electron addition and removal, chalcogen exchange, or the effect of the ligand attached to the Co atom. Our experimental findings coupled with theoretical calculations at the DFT[38,39] level provide new insights into the nature of bonding for these Mo_3CoQ_4 (Q = S, Se) complexes.

Experimental Section

General Procedures. All reactions were carried out under a nitrogen atmosphere using standard Schlenck techniques. The molecular triangular cluster $[Mo_3Se_4(dmpe)_3Cl_3]PF_6$ was prepared according to literature methods (dmpe = 1,2-bis(dimethylphosphanyl)ethane).[29] The tetraphenylborate $[Mo_3Se_4(dmpe)_3Cl_3]BPh_4$ salt was prepared by addition of an excess of $NaBPh_4$ to methanol solutions of $[Mo_3Se_4(dmpe)_3Cl_3]PF_6$ precipitating the desired compound. The remaining reactants were obtained from commercial sources and used as received. Solvents for synthesis were dried and degassed by standard methods before use.

^{31}P NMR spectra were recorded on a Varian MERCURY 300 MHz spectrometer, using CD_2Cl_2 as a solvent, and are referenced to external 85% H_3PO_4. IR spectra were recorded on a Perkin-Elmer System 2000 FTIR using KBr pellets. Cyclic voltammetry experiments were performed with a Echochemie Pgstat 20 electrochemical analyzer. All measurements were carried out with a conventional three-electrode configuration consisting of platinum working and auxiliary electrodes and a Ag/AgCl reference electrode containing aqueous 3 M KCl. The solvent used in all experiments was CH_2Cl_2 (Merck HPLC-grade). The supporting electrolite was 0.1 M tetrabutylammonium hexafluorophosphate. $E_{1/2}$ values were determined as $\frac{1}{2}(E_a + E_c)$, where E_a and E_c are the anodic and cathodic peak potentials, respectively. All potentials reported were not corrected for the junction potential. Electrospray mass spectra were recorded on a Micromass Quattro LC instrument using dichloromethane as the solvent. A capillary voltage of 3.5 kV was used in the positive scan mode, and the cone voltage (U_c) was set to 30 V to control the extent of fragmentation of the identified ions. Magnetic susceptibility measurements were made on a Quantum Design SQUID magnetometer in an applied field of 500 G between 2 and 300 K for **2** and [**2**](TCNQ)·CH_2Cl_2 (TCNQ = 7,7,8,8-tetracyanoquinomethane).

$[Mo_3(CoCO)Se_4(dmpe)_3Cl_3]$ (1). $[Mo_3Se_4(dmpe)Cl_3]BPh_4$ (130 mg, 0.1 mmol) and $CoCl_2$ (40 mg, 0.3 mmol) were dissolved in 20 mL of a solution of THF/MeOH (8:1). $NaBH_4$ (20 mg, 0.5 mmol) was added under a CO (1 atm) atmosphere, and the reaction mixture was stirred for 1 h at room temperature. The solution turned brown after 30 min. The addition of 30 mL of ether caused the complete precipitation of a brown solid, which was washed with THF (3 × 2 mL) and diethylether. The resulting solid was redissolved in CH_2Cl_2 and filtered in order to eliminate the inorganic salts from $NaBH_4$. Diethylether was layered on this solution to afford brown cubic crystals of the title compound (20 mg, 20%). Elem anal. for $C_{19}H_{48}OP_6Cl_3Se_4CoMo_3$, found: C, 18.56; H, 3.60. Required: C, 18.29,; H, 3.88. ν_{max}/cm^{-1} 1926 (C═O). ^{31}P NMR (121.47 MHz, 25 °C): δ 29.3 (d, $^2J_{P-P}$ = 11 Hz), 19.3 (d, $^2J_{P-P}$ = 11 Hz). Electrospray-MS (U_c = 30 V): *m*/*z* (CH_2Cl_2) 1255 $(M)^+$. CV (*E* vs Ag/AgCl): $E_{1/2}$ ($\mathbf{1}^+/\mathbf{1}$) = 0.18 V.

$[Mo_3(CoCl)Se_4(dmpe)_3Cl_3]$ (2). $[Mo_3Se_4(dmpe)_3Cl_3]BPh_4$ (130 mg, 0.1 mmol) and $CoCl_2$ (30 mg, 0.24 mmol) were dissolved in 20 mL of a solution of THF/MeOH (8:1). $NaBH_4$ (12 mg, 0.36 mmol) was added, and the reaction mixture was stirred for 1 h at room temperature. The solution turned brown after 30 min. The workup procedure was identical to that described for compound **1** to afford brown cubic crystals of the title compound (28 mg, 21%). Elem anal. for $C_{18}H_{48}P_6Cl_4Se_4CoMo_3$ found: C, 17.96; H, 3.96. Required: C, 17.23; H, 3.86. Electrospray-MS (U_c = 30 V): *m*/*z* (CH_2Cl_2) 1262 $(M)^+$. CV (*E* vs Ag/AgCl): $E_{1/2}$ ($\mathbf{2}^+/\mathbf{2}$) = −0.15 V.

$[Mo_3(CoCl)Se_4(dmpe)_3Cl_3]$[TCNQ] ([2]TCNQ). To a brown solution of **2** (25 mg, 0.02 mmol) in CH_2Cl_2 was added 7,7,8,8-tetracyanoquinomethane, TCNQ (6 mg, 0.04 mmol), under nitrogen, and the mixture was stirred for 30 min. The color of the solution turned green immediately. The resulting solution was filtered, and ether was layered to give green needle crystals (27 mg, 92%) suitable for X-ray analysis, which were washed with toluene and ether. Elem anal. for $C_{42}H_{68}BP_6Cl_4Se_4CoMo_3$ found: C, 24.40; H, 3.48; N, 3.89. Required: C, 24.70; H, 3.59; N, 3.84). $\nu_{\mu ax}/cm^{-1}$: 2051 (C≡N). Electrospray-MS (U_c = 30 V): *m*/*z* (CH_2Cl_2) 1262 (M^+).

X-Ray Crystallographic Study. The crystals are air-stable and were mounted on the tip of a glass fiber with the use of epoxy cement. X-ray diffraction experiments were carried out on a Bruker SMART CCD diffractometer using Mo Kα radiation (λ = 0.710 73 Å) at room temperature. Data were collected with a frame width of 0.3° in ω and a counting time of 25 s per frame for all compounds at a crystal-to-detector distance of 4 cm. The diffraction frames were integrated using the SAINT package and corrected for absorption with SADABS.[40,41] The structures were solved by direct methods and refined by the full-matrix method based on F^2 using the SHELXTL software package.[42] The crystal parameters and basic information relating data collection and structure refinement for compounds **1**·½CH_2Cl_2, **2**·CH_2Cl_2, and [**2**][TCNQ]·CH_2Cl_2 are summarized in Table 1.

Compounds **1**·½CH_2Cl_2 and **2**·CH_2Cl_2 are isostructural and crystallize in the chiral space group *R*3*c* with absolute structure parameters being refined as 0.436(16) and 0.05(2). Compound [**2**](TCNQ)·CH_2Cl_2 crystallizes in the monoclinic *P*2(1)/*n* space group. In all of the compounds, the non-hydrogen atoms were refined anisotropically while the positions of all hydrogen atoms in the diphosphane ligands and counteranions were generated geometrically, assigned isotropic thermal parameters, and allowed to ride on their respective parent carbon atoms. Dichloromethane molecules of crystallization were found in the last Fourier map in compounds **1**·½CH_2Cl_2, **2**·CH_2Cl_2, and [**2**](TCNQ)·CH_2Cl_2, which were refined isotropically. The solvent hydrogen atoms were not included in the refinement.

Computational Methods

All calculations were carried out using the ADF 2005 program.[43] All species studied were optimized starting from the X-ray structure using DFT calculations, in particular, the BP86 generalized gradient

(38) Dreizler, R. M.; Gross, E. K. U. *Density Functional Theory: An Approach to the Quantum Many-Body Problem*; Springer: Berlin, 1990.
(39) Parr, R.; Yang, W. *Density-Functional Theory of Atoms and Molecules*; Oxford University Press: New York, 1989.
(40) *SAINT*, v. 5.0; Bruker Analytical X-Ray Systems: Madison, WI, 1996.
(41) Sheldrick, G. M. *SADABS empirical absorption program*; University of Göttingen: Göttingen, Germany, 1996.
(42) Sheldrick, G. M. *SHELXTL*, v. 5.1; Bruker Analytical X-Ray Systems: Madison, WI, 1997.
(43) Velde, G. T.; Bickelhaupt, F. M.; Baerends, E. J.; Guerra, C. F.; Van Gisbergen, S. J. A.; Snijders, J. G.; Ziegler, T. *J. Comput. Chem.* **2001**, *22*, 931.

Table 1. Crystallographic Data for $[Mo_3(CoCO)Se_4(dmpe)_3Cl_3]\cdot 0.5CH_2Cl_2$ (**1**·0.5CH_2Cl_2), $[Mo_3(CoCl)Se_4(dmpe)_3Cl_3]\cdot CH_2Cl_2$ (**2**·CH_2Cl_2), and $[Mo_3(CoCl)Se_4(dmpe)_3Cl_3](TCNQ)\cdot CH_2Cl_2$ [**2**](TCNQ)·CH_2Cl_2)

compound	**1**·½CH_2Cl_2	**2**·CH_2Cl_2	[**2**](TCNQ)·CH_2Cl_2
empirical formula	$C_{19.50}H_{49}Cl_4CoMo_3OP_6Se_4$	$C_{19}H_{50}Cl_6CoMo_3P_6Se_4$	$C_{31}H_{54}Cl_6CoMo_3N_4P_6Se_4$
fw	1289.80	1339.60	1540.87
cryst syst	hexagonal	hexagonal	monoclinic
a, Å	15.8529(4)	15.828(2)	10.587(3)
b, Å			26.935(7)
c, Å	29.2944(16)	29.060(8)	18.952(5)
β, deg			103.458(7)
V, Å^3	6375.8(4)	6305(2)	5256(3)
T, K	293(2) K	293(2) K	293(2) K
space group	*R*3*c*	*R*3*c*	P2(1)/n
Z	6	6	4
μ(Mo Kα), mm^{-1}	5.167	5.351	4.296
reflns collected	11334	11264	29870
φ range for data collection	2.03 to 25.00°	2.04 to 25.00°	1.51 to 25.00°
unique reflns/*R*(int)	2486 [*R*(int) = 0.0791]	2228 [*R*(int) = 0.1299]	9255 [*R*(int) = 0.1169]
GOF on F^2	1.027	1.002	0.996
R1[a]/wR2[b]	R1 = 0.0431, wR2 = 0.0952 R1 = 0.0639 wR2 = 0.1034	R1 = 0.0533, wR2 = 0.1095 R1 = 0.0890, wR2 = 0.1244	R1 = 0.0551, wR2 = 0.1176 R1 = 0.1238, wR2 = 0.1458
residual ρ/e A^{-3}	0.779 and −0.865	1.026 and –0.950	0.826 and –1.111

[a] $R1 = \sum||F_0| - |F_c||/\sum F_0$. [b] $wR2 = [\sum[w(F_0^2 - F_0^2)^2]/\sum[w(F_0^2)^2]]^{1/2}$.

Scheme 1. (i) $CoCl_2/NaBH_4/CO$, (ii) $CoCl_2/NaBH_4$, and (iii) TCNQ; the Environment around One Molybdenum Site Is Illustrated for Clarity

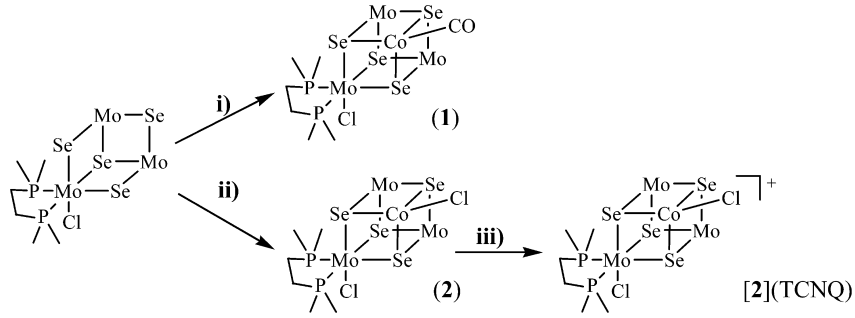

approximation, triple-ξ plus polarization Slater-type orbital basis sets[44,45] (BP86/VTZP), and a fine mesh for numerical integration of the matrix elements. Large frozen cores (Mo.4p, Co.3p, Se.3p, Cl.2p, S.2p, P.2p, and C.1s) were employed. Relativistic effects are considered using the ZORA formalism.[46–48] For open-shell species, the unrestricted methodology was employed, the calculated $<S^2>$ values being in excellent agreement with the theoretically expected values.

Results and Discussion

Synthesis and Electrochemical and Magnetic Properties. The [3 + 1] building block strategy has proven to be the most efficient route to construct cuboidal complexes with a $Mo_3M'S_4$ (M′ = transition metal) core in both aqueous and organic media.[49–51] In these reactions, the preassembled Mo_3 trinuclear complex is typically reacted with a second M′-containing reagent to afford the desired compound. This approach has been successfully used in our group to prepare a series of cluster complexes with a Mo_3CoS_4 core bearing diphosphane ligands.[22] In the present work, we study the possibility of extending this synthetic strategy to prepare the homologue selenium-containing clusters with a Mo_3CoSe_4 core. The synthetic routes are summarized in Scheme 1.

The reaction of $[Mo_3Se_4(dmpe)_3Cl_3]^+$ with $CoCl_2$ in the presence of carbon monoxide and an excess of sodium borohydride in THF/CH_3OH mixtures gives the neutral 16-metal-electron cluster $[Mo_3(CoCO)Se_4(dmpe)_3Cl_3]$ (**1**). When the reaction is done in the absence of CO, the also neutral 15-metal-electron cluster $[Mo_3(CoCl)Se_4(dmpe)_3Cl_3]$ (**2**) is obtained. In both cases, the desired products precipitate from the reaction mixture, which ultimately facilitates the workup procedure. Compound **2** is quantitatively oxidized to the 14-metal-electron $[\mathbf{2}]^+$ cation by treatment with equimolar amounts of TCNQ to afford the charge transfer salt [**2**](TCNQ). All compounds have been characterized by electrospray ionization (ESI) mass spectrometry. Despite the neutral nature of complexes **1** and **2**, they can be readily ionized in the ESI chamber to give abundant signals due to the $\mathbf{1}^+$ and $\mathbf{2}^+$ molecular peaks. This ionization mode is unusual as compared with other neutral halide metal complexes, where the loss of one halide ligand or adduct formation appear to be the dominant ionization processes.[28,52]

(44) Becke, A. D. *Phys. Rev. A: At., Mol., Opt. Phys.* **1988**, *38*, 3098.
(45) Perdew, J. P. *Phys. Rev. B: Condens. Matter Mater. Phys.* **1986**, *33*, 8822.
(46) Vanlenthe, E.; Baerends, E. J.; Snijders, J. G. *J. Chem. Phys.* **1993**, *99*, 4597.
(47) Vanlenthe, E.; Baerends, E. J.; Snijders, J. G. *J. Chem. Phys.* **1994**, *101*, 9783.
(48) Vanlenthe, E.; Snijders, J. G.; Baerends, E. J. *J. Chem. Phys.* **1996**, *105*, 6505.
(49) Hidai, M.; Kuwata, S.; Mizobe, Y. *Acc. Chem. Res.* **2000**, *33*, 46.
(50) Hernandez-Molina, R.; Sokolov, M. N.; Sykes, A. G. *Acc. Chem. Res.* **2001**, *34*, 223.
(51) Llusar, R.; Uriel, S. *Eur. J. Inorg. Chem.* **2003**, 1271.
(52) Henderson, W.; Evans, C. *Inorg. Chim. Acta* **1999**, *294*, 183.

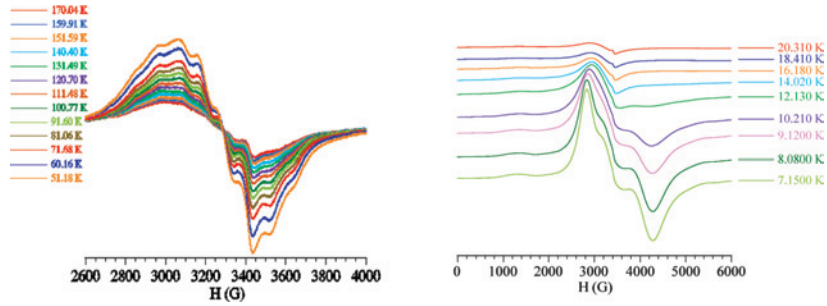

Figure 1. Variable-temperature EPR spectra of $[Mo_3(CoCl)S_4(dmpe)_3Cl_3]$ and $[Mo_3(CoCl)Se_4(dmpe)_3Cl_3]$.

For compounds **1** and **2**, the electron detachment mechanism is clearly favored in front of other ionization processes, and this feature can be explained in terms of their redox behavior. Cyclic voltammetry experiments show reversible redox processes at 0.18 V (vs Ag/AgCl) for the $\mathbf{1}^+/\mathbf{1}$ couple and −0.15 V for the $\mathbf{2}^+/\mathbf{2}$ couple. These values suggest that both redox pairs might be easily interconverted as exemplified for compounds **2** and [**2**](TCNQ). The redox processes observed for the Mo_3CoSe_4 complexes are comparable to those previously reported for their Mo_3CoS_4 sulfur homologues where a slight cathodic shift (ca. 0.05 V) is observed on going from the sulfur- to the selenium-containing compounds. We have previously reported that the S/Se exchange in their trinuclear $[Mo_3Q_4(dmpe)_3Cl_3]^+$ starting materials does not significantly affect the redox behavior.[31] More remarkable differences are observed between the redox potentials of **1** and **2**, attributed to the different cobalt coordination environments, CO for **1** and Cl for **2**, which in turn affects the metal electron count, 16 e^- for **1** and 15 e^- for **2**. Moreover, the effect of the ligand coordinated to the heterometal strongly influences the electronic structure of these Mo_3CoQ_4 (Q = S or Se) complexes, as will be analyzed in the following subsections.

Harris et al.[53] have proposed a theoretical scheme for these $Mo_3M'S_4$ (M′ = Co, Ni, Pd, Sn) clusters with 14 to 16 metal electrons, where two or four electrons partially or fully occupy the highest occupied molecular orbital (HOMO) orbital with an "e" symmetry. Support to this MO scheme is given by the magnetic properties previously reported for the series of Mo_3CoS_4 clusters.[22] Aimed at validating whether this model is also applicable to the homologous Mo_3CoSe_4 series, a detailed analysis of the magnetic properties of compounds **1**, **2**, and [**2**](TCNQ) is carried out. Magnetic susceptibility measurements for **2** reveal a similar behavior to that previously observed for the sulfur compound $[Mo_3(CoCl)S_4(dmpe)_3Cl_3]$ with a magnetic moment of 1.71 μ_B at room temperature in agreement with an $S = ½$ ground state. The $1/\chi$ plot shows typical Curie–Weiss behavior, with a small value for θ (−0.37 K). The magnetic properties of the charge transfer salt [**2**](TCNQ) have also been investigated in the 2–300 K range. In compound [**2**](TCNQ), the value of the χT product (1.1 emu K/mol) remains largely unchanged in the 20–300 K range. This behavior agrees with the presence of an $S = 1$ cluster while the $TCNQ^-$ does not contribute to the total magnetic susceptibility. This observation differs from the magnetic data reported for the sulfur analogue where two independent magnetic moieties, one based on the heterodimetallic Mo_3CoS_4 cuboidal cluster sublattice and the other on the organic acceptor TCNQ, coexist, although no cooperative phenomena have been observed. Both [**2**](TCNQ) and $[Mo_3(CoCl)S_4(dmpe)_3Cl_3]$(TCNQ) are isostructural, so only very subtle changes are observed for the contacts within the TCNQ sublattice and between the organic and inorganic substructures. This fact has made all attempts to rationalize differences in magnetic behavior between these two TCNQ phases unproductive. In both cases, at temperatures below 15 K, the χT product decreases sharply, indicative of antiferromagnetic interactions and/or zero field splitting (ZFS) in the $S = 1$ cation. Let us note that distinctive magnetic contributions of the TCNQ acceptor have also been reported for hybrid charge transfer salts based on isomeric methylpyridinium-substituted verdazyl radicals.[54]

The spin ground state of compounds **1**, **2**, and [**2**](TCNQ) is further confirmed by the X-band electron paramagnetic resonance (EPR) experiments, which show that **1** and [**2**](TCNQ) are EPR-silent, as expected for compounds with $S = 0$ and $S = 1$, respectively. In contrast, **2** exhibits an anisotropic signal centered at $g \approx 2.05$ with paramagnetic behavior in the temperature range 5–300 K, which is consistent with the $S = {}^1/_2$ ground spin state. For comparative purposes, the EPR spectra of compound **2** together with the sulfur homologue $[Mo_3(CoCl)S_4(dmpe)_3Cl_3]$ are shown in Figure 1.

While in the spectrum of $[Mo_3(CoCl)S_4(dmpe)_3Cl_3]$ a hyperfine structure with eight signals can clearly be observed at intermediate temperatures, the hyperfine structure for **2** is only visible at very low temperatures (20 K onward), and only four signals can be resolved. This is concurrent with a small increase in the g value for the Se-containing cluster. Both effects, the shift of the g value to higher values and the loss of resolution, can be attributed to the expected greater spin–orbit contribution of selenium.[55] Both the splitting pattern and the hyperfine coupling constant are typical of the $^{59}Co^{2+}$ ion ($I = {}^7/_2$), indicating that the unpaired electron density is located mainly around the cobalt ion. This is in contrast with results reported for the 17-electron cluster

(53) Bahn, C. S.; Tan, A.; Harris, S. *Inorg. Chem.* **1998**, *37*, 2770.
(54) Mukai, K.; Jinno, S.; Shimobe, Y.; Azuma, N.; Taniguchi, M.; Misaki, Y.; Tanaka, K. K. I.; Hosokoshic, Y. *J. Mater. Chem.* **2003**, 1614.
(55) Bestari, K.; Cordes, A. W.; Oakley, R. T.; Young, K. M. *J. Am. Chem. Soc.* **1990**, *112*, 2249.

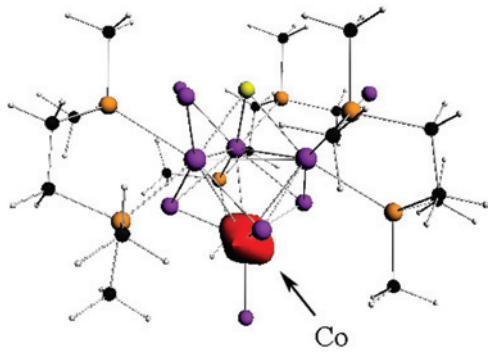

Figure 2. Isocontour plot of unpaired electron density for **2** calculated at the DFT level (cutoff value 0.02).

$[Mo_3CuS_4(H_2O)_{10}]^{4+}$,[56] but in very good agreement with the spin polarization calculated by spin-unrestricted DFT methods shown in Figure 2, where the unpaired electron is fully located on the Co atom. Further analysis on the electronic structure arising from the theoretical calculations will be presented in the next subsection.

Molecular and Electronic Structure. The isolation of complexes **1**, **2**, and $\mathbf{2}^+$ with 16, 15, and 14 metal electrons, respectively, provides an ideal system to experimentally analyze the nature of the frontier orbitals of these complexes on the basis of structural results. For that reason, the crystal structures of compounds $\mathbf{1}\cdot\frac{1}{2}CH_2Cl_2$, $\mathbf{2}\cdot CH_2Cl_2$, and [**2**](TCNQ)$\cdot CH_2Cl_2$ have been determined by X-ray single-crystal diffraction analysis. All three compounds possess a Mo_3CoSe_4 cubane-type cluster core, as exemplified in Figure 3 for compounds **1** and **2** and also applicable to the $\mathbf{2}^+$ cation.

The cluster core consists of a slightly distorted tetrahedral arrangement of one cobalt and three molybdenum atoms. Each tetrahedral face is capped by a μ_3-coordinated selenium atom, thus generating a cubanelike structure. Each molybdenum atom presents a pseudo-octahedric coordination environment, with two out of three external positions being occupied by the phosphorus atoms of the dmpe ligand, one trans to the (μ_3-Se(1)) and another trans to the (μ_2-Se(2)). The third position is occupied by a chlorine atom which is situated trans to the remaining (μ_2-Se(2)). The cobalt atom presents a pseudotetrahedric environment defined by three Se atoms and a CO group for **1** and one chlorine atom for **2** and $\mathbf{2}^+$. A comparison between the main bond distances for compounds $\mathbf{1}\cdot\frac{1}{2}CH_2Cl_2$, $\mathbf{2}\cdot CH_2Cl_2$, and [**2**](TCNQ)$\cdot CH_2Cl_2$ is collected in Table 2. For comparative purposes, the geometric features of the sulfur homologues are also included to analyze the structural consequences of the chalcogen exchange.

The replacement of sulfur by selenium mainly affects the bond distances within the Mo_3CoQ_4 cuboidal core. An increase of ca. 0.06 Å in the Mo−Mo and Mo−Co bond distances is ascribed to the increased atomic radius of selenium, which consequently expands the cuboidal core. Noticeably, the tendencies in the Mo−Mo and Mo−Co bond distances upon variation of the electronic population are quite similar for the Mo_3CoS_4 and Mo_3CoSe_4 series. The analogy observed between the change in bond length associated with the removal of one electron to afford the 14-electron species $[\mathbf{2}]^+$ and $[Mo_3(CoCl)S_4(dmpe)_3Cl_3]^+$ indicates that the change of selenium for sulfur has no significant effect on the electronic structure of the cluster. Either for the series of sulfur and selenium complexes, these experimental observations agree with the entering electrons occupying an orbital which is basically Mo−Mo nonbonding, slightly Mo−Co bonding, and Co−Cl antibonding.

Theoretical Analysis of the Molecular Orbital Diagram. With the aim of rationalizing the experimental consequences of the different metal countings and the presence of different cluster Mo_3CoQ_4 (Q = S, Se) cores on the 14-, 15-, and 16-electron species, a DFT study on these structures has been carried out at the BP86/VTZP level. The available experimental geometries and their behavior upon the addition/removal of electrons are well reproduced by DFT calculations. The type and composition of the molecular orbitals do not change for the 14-, 15-, and 16-electron complexes. Hence, the HOMO for the 16-electron complex corresponds to two fully occupied degenerate e-symmetry orbitals (2e) yielding a singlet ground state of C_3 symmetry. Correspondingly, the 15-electron complex presents a doublet ground state, and a triplet ground state is found for the 14-electron complex. Comparison of S and Se clusters yields nearly identical MO schemes. However, important differences on the HOMOs are found between **1** and **2**, which will be discussed in detail here and related to the experimental findings previously described. The bonding in $Mo_3(CoCO)S_4$ complexes was early studied by Harris et al.,[53] and the "2e" orbitals of complex **1** plotted in Figure 4a and b are in excellent agreement with their scheme. However, complex **2** presents "2e" MOs (see Figure 4c and d) with different atomic orbital compositions, pointing out the important role of the ligand attached to the Co atom in the nature of the HOMO, a fact which was not taken into consideration in early bonding models.

In Table 3, the atomic and orbital contributions to the 2e MOs for complexes **1** and **2** are collected. For complex **1**, the 2e MOs are almost equally distributed between the atoms forming the $Mo_3Se_4(dmpe)_3Cl_3$ cluster (55%) and the Co−CO moiety (45%). Meanwhile, the 2e orbitals of **2** are distributed 74% on the CoCl atoms (~65% Co and 9% Cl) and 26% on the cluster (7% bridging Se, 15% Mo atoms) showing π-type antibonding character between Co and Cl atoms and slightly bonding character between Co and Mo atoms (see Figure 4c and d). In order to understand this difference, it is convenient to analyze the orbital contributions to these atomic percentages. The Co participates with different d orbitals of the 2e MOs of complexes **1** and **2**. For complex **1**, the d_{xy} and $d_{x^2-y^2}$ orbitals of the Co atom have the largest contributions (34% for each e orbital, respectively), whereas for complex **2** the d_{yz} and d_{xz} are the main contributing d orbitals (46% for each e orbital, respectively).

The different compositions of the 2e MOs can be rationalized in terms of the decomposition of the MO diagram into interacting fragments (see Figure 5), namely, the $Mo_3Se_4(dmpe)_3Cl_3$ cluster and the ··CoCO·· and ··CoCl·· fragments

(56) Miyamoto, R.; Kawata, S.; Iwaizumi, M.; Akashi, H.; Shibahara, T. *Inorg. Chem.* **1997**, *36*, 542.

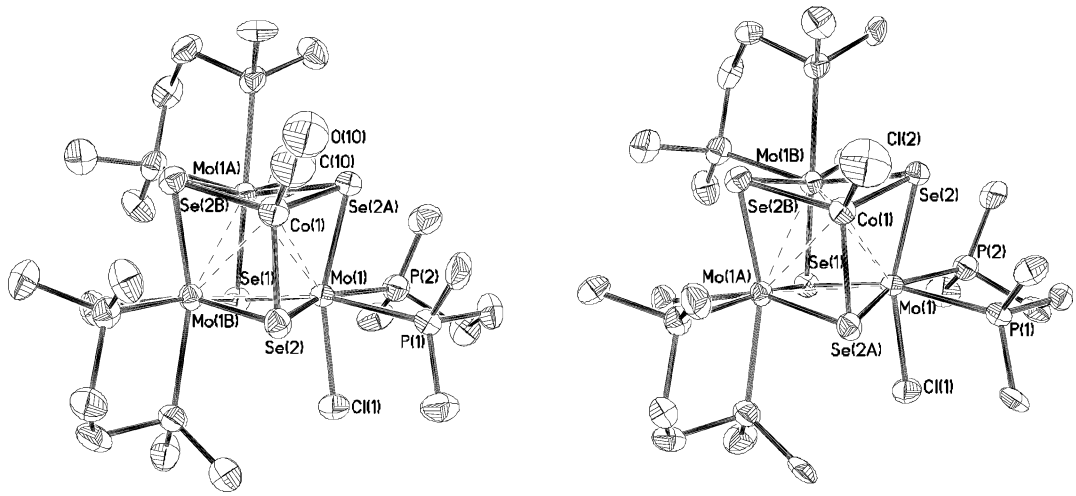

Figure 3. ORTEP representation (50% probability ellipsoids) and numbering scheme for compounds **1** (left) and **2** (right).

Table 2. Selected Bond Distances for Compounds **1**, **2**, and [**2**]TCNQ and Their Sulfur Homologues[a]

dist. (Å)	**1**/$[Mo_3(CoCO)S_4(dmpe)_3Cl_3]$	**2**/$[Mo_3(CoCl)S_4(dmpe)_3Cl_3]$	$[\mathbf{2}]^+$ $[Mo_3(CoCl)S_4(dmpe)_3Cl_3]^+$
Mo−Mo	2.8704(15)/2.8028(14)	2.866(2)/2.8079(12)	2.848[5]/2.782[7]
Mo−Co	2.742(2)/2.673(2)	2.765(3)/2.707(2)	2.816[12]/2.760[14]
Mo−Cl	2.552(3)/2.542(2)	2.529(4)/2.530(2)	2.492[5]/2.473[4]
Co−Cl/Co−C	1.84(3)/1.93(4)	2.221(9)/2.240(4)	2.160(3)/2.164(4)

[a] Averaged values are given in brackets.

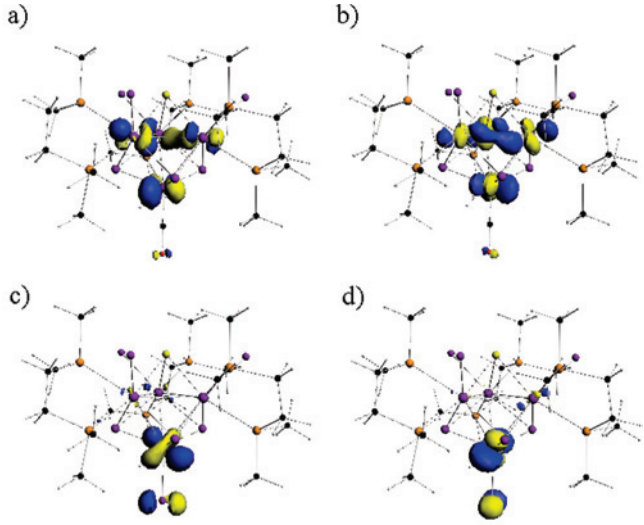

Figure 4. Isocontour plot of degenerate 2e MOs for complexes **1** (a,b) and **2** (c,d).

for complexes **1** and **2**, respectively. Interestingly, the ··CoCO·· fragment has a different orbital ordering than the ··CoCl·· one, due to the stabilization of the Π_x and Π_y orbitals by the backdonation from the d_{xz} and d_{yz} occupied orbitals of the Co atom into the π_x and π_y antibonding orbitals of the carbonyl ligand, in agreement with previous descriptions in the literature for sulfur clusters.[53] On the other hand, the chlorine atom cannot accept the backdonation from the Co d_{xz} and d_{yz} occupied orbitals due to the lack of empty p orbitals, and the energy of Π_x and Π_y orbitals is shifted up with respect to the $\Delta_{x^2-y^2}$ and Δ_{xy} orbitals, leading to an orbital inversion between the two sets of e symmetry orbitals of the respective complexes, as shown in Figure 5. Hence, the 2e MOs of complexes **1** and **2** correspond to different atomic orbitals. The 2e MOs of complex **1** have some bonding character between the Mo and the Co atoms, while the 2e MO of complex **2** is localized on the ··CoCl·· fragment having some π^* character. The MO diagram described for complex **2** fits perfectly into the geometrical changes observed; the Co−Cl distance is elongated, and the Co−Mo distance is shortened upon reduction from the 14-electron to the 15-electron system, in agreement with the overlap between atomic orbitals forming the degenerate 2e MOs. Also, the EPR data of the 15-electron **2** cluster (see above) are nicely complemented by the MO diagram, since the localization of the unpaired electron on the Co atom is in perfect agreement with the localized nature of the 2e molecular orbital.

Conclusions

The preparation of the cluster series $[Mo_3(CoCO)Se_4(dmpe)_3Cl_3]$ (**1**), $[Mo_3(CoCl)S_4(dmpe)_3Cl_3]$ (**2**), and $[Mo_3(CoCl)S_4(dmpe)_3Cl_3](TCNQ)$ ([**2**](TCNQ)) with three different metal electron populations has been carried out by adaptation of the previously reported synthetic routes for the sulfur homologues. A comparison of the electrochemical, magnetic, and geometric features of the complexes with different cluster core Mo_3CoQ_4 (Q = S, Se) compositions and electron counting is carried out. The electrochemical properties do not vary significantly upon chalcogen exchange, and magnetic measurements indicate similar ground-state configurations for the isoelectronic Mo_3CoQ_4 (Q = S, Se) cluster complexes. However, S/Se exchange in the hybrid charge transfer salts formulated as $[Mo_3(CoCl)Q_4(dmpe)_3Cl_3](TCNQ)$ (Q = S, Se) has a dramatic effect on the contribution of the organic acceptor to magnetic properties. Despite the origin of such differences not being clear at present, we experimentally observe that the replacement of the Mo_3CoS_4 by the larger Mo_3CoSe_4 core produces $TCNQ^-$

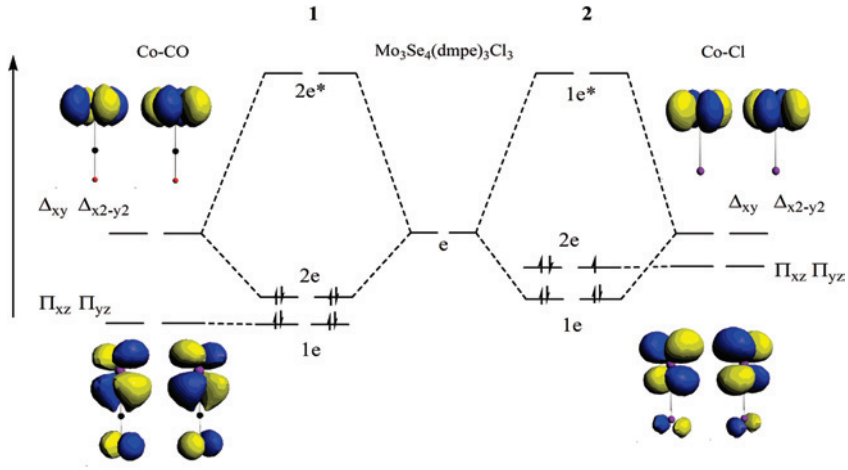

Figure 5. Qualitative interaction MO diagram for complexes **1** and **2** in terms of the $Mo_3Se_4(dmpe)_3Cl_3$ cluster (center) and "CoCO" (left) or "CoCl" (right) fragments. The occupation of the 2e MO is of two, three, and four electrons for the 14-, 15-, and 16-electron clusters, respectively. For clarity, only the "e" symmetry orbitals have been considered.

Table 3. BP86/TZP Calculated Atomic and Orbital Contributions to the 2e Molecular Orbitals of Complexes **1** and **2** for the 16-Electron Species

complex	orbital	atomic contrib. (%)				orbital contrib. (%)					
1	2e (1)	41	Co	27	d_{xy}	9	$d_{x^2-y^2}$	4	d_{yz}		
Co-CO		4	CO	2	p_y (C)	2	p_y (O)				
		36	$Mo_{1,2,3}$	8	$d_{x^2-y^2}(Mo_1)$	8	$d_{xy}(Mo_2)$	6	$d_{xy}(Mo_3)$	5	$d_{yz}(Mo_1)$
		5	$Se_{1,2,3}$	2	dy (Se_1)	2	p_y (Se_2)	2	p_y (Se_3)		
	2e (2)	41	Co	27	$d_{x^2-y^2}$	9	d_{xy}	4	d_{xz}		
		4	CO	2	p_x (C)	2	p_x (O)				
		37	$Mo_{1,2,3}$	8	$d_{x^2-y^2}$	7	$d_{x^2-y^2}$	6	$d_{x^2-y^2}$		
		6	Se	2	p_x (Se1)	2	p_x (Se2)	2	p_x (Se3)		
2	2e (1)	66	Co	35	d_{yz}	15	$d_{x^2-y^2}$	11	d_{xz}	4	d_{xy}
Co−Cl		9	Cl	7	p_y	2	p_x				
		5	$Mo_{1,2,3}$	2	$d_{x^2-y^2}$	2	$d_{x^2-y^2}$	1	$d_{x^2-y^2}$		
		7	Se	5	p_y						
	2e (2)	66	Co	35	d_{xz}	15	d_{xy}	11	d_{yz}	4	$d_{x^2-y^2}$
		9	Cl	7	p_x	2	p_y				
		5	$Mo_{1,2,3}$	2	d_{xy} (Mo_1)	2	$d_{xz}(Mo_2)$	1	$d_{xz}(Mo_3)$		
		7	Se	2	p_x (Se_1)	2	p_x (Se_2)	2	p_x (Se_3)		

radical anions with a triplet and singlet ground state, respectively. The sulfur/selenium exchange within the Mo_3CoQ_4 series essentially elongates the Mo−Mo and Mo−Co bond distances as a consequence of the increased atomic radius of selenium, which represents an expansion of the cuboidal cluster core. However, the variations in the Mo−Mo and Mo−Co bond distances upon variation of the electronic population are quite similar for the Mo_3CoS_4 and Mo_3CoSe_4 series. This experimental evidence is rationalized on the basis of the electronic structure analysis obtained by means of DFT calculations. The HOMO for the $[Mo_3(CoCO)Se_4(dmpe)_3Cl_3]$ cluster is composed of Co and Mo atomic orbitals, while the $[Mo_3(CoCl)Se_4(dmpe)_3Cl_3]$ cluster is formed by Co and Cl atoms displaying π^* character. These differences are related to the relative energies of the Co−ligand fragment with regard to the $[Mo_3Se_4(dmpe)_3Cl_3]^+$ energy and are a direct consequence of the absence or presence of ligand-to-metal π backdonation found for the Co−Cl and Co−CO units. The electronic structure of these heterobimetallic clusters is then determined by the nature of the ligand attached to the Co. The insights obtained from the proposed MO diagram are in excellent agreement with the structural and magnetic investigations on these complexes.

Acknowledgment. This work was supported by the Spanish Ministerio de Educación y Ciencia (MEC) and EU FEDER (Project CTQ2006-15447-C02-01), Generalitat Valenciana (Projects GV/2007/106 and ACOMP/2007/286), and Fundació Bancaixa-Universitat Jaume I (Projects P1.1B2004-19 and P1.1A2007-12) . V.P. and A.A. acknowledge support from the MEC by the JdC and RyC programs, respectively. The authors also are grateful to the Servei d'Informatica and the Serveis Centrals d'Instrumentació Científica (SCIC) of the Universitat Jaume I for providing us with computing time and spectroscopic facilities. This work is dedicated to the memory of Professor F. Albert Cotton.

Supporting Information Available: A table comparing experimental (as reported in Table 2) and optimized (using BP86/VTZP methodologies) bond distances for clusters **1**, **2**, and $[\mathbf{2}]^+$ is included. The Cartesian coordinates for these clusters obtained from the BP86/VTZP optimization are also listed. Crystallographic data (excluding structure factors) for the structures reported in this paper can be obtained free of charge at http://pubs.acs.org.

IC7022083